Towards Multi-Modal Image-Guided Tumour Identification in Robot-Assisted Partial Nephrectomy

Ghassan Hamarneh[1], Alborz Amir-Khalili[2], Masoud S. Nosrati[1], Ivan Figueroa[2], Jeremy Kawahara[1], Osama Al-Alao[4], Jean-Marc Peyrat[3], Julien Abi-Nahed[3], Abdulla Al-Ansari[4], and Rafeef Abugharbieh[2]

***Abstract*— Tumour identification is a critical step in robot-assisted partial nephrectomy (RAPN) during which the surgeon determines the tumour localization and resection margins. To help the surgeon in achieving this step, our research work aims at leveraging both pre- and intra-operative imaging modalities (CT, MRI, laparoscopic US, stereo endoscopic video) to provide an augmented reality view of kidney-tumour boundaries with uncertainty-encoded information. We present herein the progress of this research work including segmentation of pre-operative scans, biomechanical simulation of deformations, stereo surface reconstruction from stereo endoscopic camera, pre-operative to intra-operative data registration, and augmented reality visualization.**

I. INTRODUCTION

Surgery remains one of the primary methods for terminating cancerous tumours. Minimally-invasive robotic surgery, in particular, provides several benefits including filtering of hand tremor, offering more complex and flexible manipulation capabilities that lead to increased dexterity and higher precisions, three-dimensional view of the surgical scene, and more comfortable seating for the surgeon. This in turn leads to reduced blood loss, lower infection and complication rates, less post-operative pain, shorter hospital stays and better overall surgical outcomes [1].

Medical imaging plays an important role both before and during surgeries. In image-guided interventions, pre-operative 3D medical imaging modalities, mainly computed tomography (CT) and magnetic resonance imaging (MRI), are used for surgical planning [2]. During this stage, tumour localization and resection margins are meticulously identified to remove cancerous tissues while sparing healthy tissue. However, transferring such plans from the pre-operative frame-of-reference to the dynamic intra-operative scene remains a necessary yet largely unsolved problem. To address this problem, many state-of-the-art methods rely on manual rigid alignment of pre-operative segmentation to intra-operative stereo data (after stereo surface reconstruction) followed by motion tracking [3], [4], [5]. Other works focus on projecting 3D pre-operative data directly onto 2D intra-operative data, especially with intra-operative 2D X-ray and 2D ultrasound [6]. Recent methods incorporate biomechanical models to predict realistic deformation for use in non-rigid registration as this has proven to enhance registration accuracy in large deformations [7]. In addition, the use of biomechanical models can assist the registration of organs' internal structures such as vessels and tumours [8]. Augmenting the surgeons' view with these registered images is non-trivial, where some methods propose using a detailed mesh of the pre-operative model [3], while more recent works focus on selective visualization methods aimed at minimizing information overload [5].

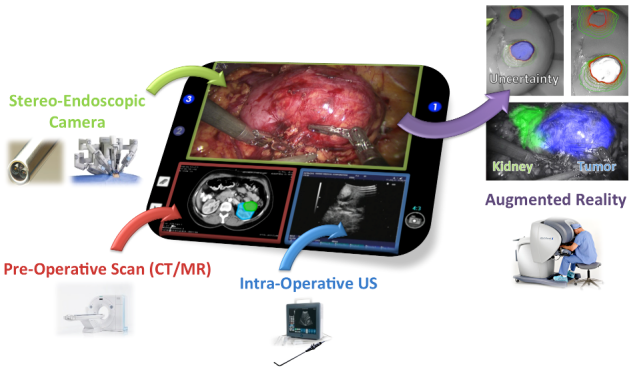

Fig. 1: Overview of our proposed image-guided navigation system for robot-assisted partial nephrectomy, in which the stereo-endoscopic view of the surgeon is augmented with kidney-tumour boundaries derived from pre- and intra-operative imaging modalities.

In this paper, we describe our team's progress towards addressing the aforementioned issues in pre-operative surgical planning, intra-operative image registration, and augmented reality visualization for image-guided tumour identification (Fig. 1 and 2), where we focused on kidney cancer cases with robot-assisted partial nephrectomy (RAPN) performed with a da Vinci surgical robot (Intuitive Surgical, Inc.).

II. PRE-OPERATIVE SURGICAL PLANNING

To help the surgeon during surgical planning, we developed a semi-automatic approach for kidney and tumour segmentation in pre-operative CT scans, which are to be transferred to the intra-operative frame-of-reference. We also investigated the biomechanical simulation of kidney and tumour deformations under external pressure load (e.g. during

[1]G. Hamarneh, M. S. Nosrati, and J. Kawahara are with the Medical Image Analysis Lab, Simon Fraser University, Burnaby, Canada {hamarneh, smn6, jkawahar}@sfu.ca

[2]R. Abugharbieh, A. Amir-Khalili, and I. Figueroa are with the Biomedical Signal and Image Computing Lab, University of British Columbia, Vancouver, Canada {rafeef, alborza, ivanf}@ece.ubc.ca

[3]J. Abi-Nahed and J.-M. Peyrat are with the Qatar Robotic Surgery Centre, Qatar Science & Technology Park, Doha, Qatar {jabinahed, jmpeyrat}@qstp.org.qa

[4]A. Al-Ansari and O. Al-Alao are with the Urology Department, Hamad Medical Corporation, Doha, Qatar {aalansari1, oalalao}@hmc.org.qa

patient insufflation) to minimize discrepancies between tissue pre- and intra-operative shapes and relative positions.

A. Pre-Operative CT Segmentation

We perform pre-operative 3D image segmentation of the tumour and surrounding healthy tissue in the CT scans using an interactive version of the random walker algorithm [9], [10], which provides a probabilistic labelling of tissues.

Let $G = (V, E)$ be a graphical representation of the pre-operative volume I_{pre} with vertices $v \in V$ and edges $e \in E \subset V \times V$. By placing a few seeds on the background and organs of interests, vertices are decomposed into marked (seeded) V_M and unmarked V_U. Having the labels set $\mathcal{L} = \{\ell_1, \cdots, \ell_n\}$, where n is the number of labels, the random walker method assigns a probability vector $\boldsymbol{p}_i = (x_i^1, \cdots, x_i^n)$ to each pixel $v_i \in V$ by solving the following system of linear equations (see [10] for more details):

$$\left(L_U + \gamma \sum_{r=1}^{n} \Lambda_U^r\right) x_U^s = \lambda_U^s - B f^s, \tag{1}$$

where $L = \begin{bmatrix} L_M & B \\ B^T & L_U \end{bmatrix}$ is the $|V| \times |V|$ graph's combinatorial Laplacian matrix, γ is a positive constant, and $\Lambda = \begin{bmatrix} \Lambda_M & 0 \\ 0 & \Lambda_U \end{bmatrix}$ is a diagonal matrix with the values of λ^s that represents the prior probability of a specific node (or voxel) belonging to class ℓ_s. Both L and Λ are decomposed into their marked (M) and unmarked (U) components. f^s is an $|V_M| \times 1$ indicator vector where $f_j^s = 1$ if x_j belongs to ℓ_s and $f_j^s = 0$ if it does not. The system of linear equations of (1) is solved for x_U^s which is the probability of unmarked nodes belonging to class ℓ_s. From these membership probabilities, we extract 3D models of kidney and tumour used in the succeeding steps.

B. Biomechanical Modeling of Tissue Deformations

To better model the intra-operative deformations, we update the pre-operative segmentation using a biomechanical model of kidney tissue and tumour that simulates deformations under the exertion of different external forces (e.g. pressure change during insufflation):

$$M\ddot{u} + C\dot{u} + Ku = F \tag{2}$$

where M, C and K are the mass, damping and stiffness matrices, respectively, F is the external force matrix applied to the system consisting of gravity and insufflation pressure over the surface of the kidney, and u is the displacement. The stiffness matrix K is built using the material parameters, Young's modulus and Poisson ratio, adopted from the literature [11]. The elements' topology is obtained from kidney and tumour 3D segmentations meshed using Gmsh[1]. We use the SOFA platform[2] to build this biomechanical model with the finite element method (FEM) using a corotational tetrahedral formulation and a Eulerian implicit solver. The output of this simulation is a prediction of kidney and tumour deformations between their pre- and intra-operative shapes that help improve the pre- to inta-operative scene registration step with a more realistic initialization [12].

[1]http://geuz.org/gmsh/

[2]http://www.sofa-framework.org/

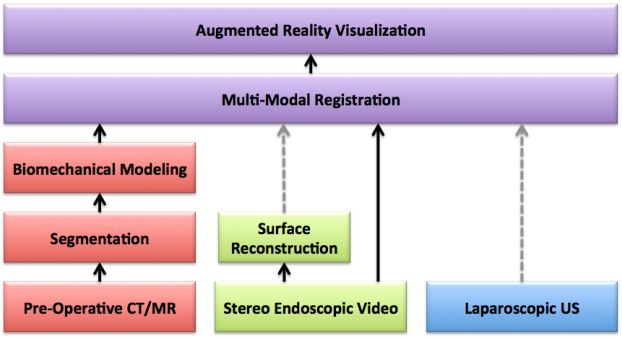

Fig. 2: Data processing and visualization workflow of our proposed image-guided navigation system (future work in grey dotted lines).

III. PRE- TO INTRA-OPERATIVE IMAGE REGISTRATION

We developed a technique for registering our pre-operative CT segmentations to the intra-operative stereo endoscopic video stream, which we use to extract the structures of the visible surfaces in the surgical scene.

A. Stereo Surface Reconstruction

We reconstruct the surface of the surgical scene from stereo endoscopic video using correlation-based dense matching of left and right camera views [13]. We implemented this step on the GPU for real-time processing [14]. The robustness of reconstruction is complicated by many factors including a small baseline between the optical centres of the cameras, presence of blood and smoke, specular highlights, occlusion, and smooth/textureless regions. In order to improve accuracy, we also regularize the reconstructed surface by incorporating pre-operative CT segmentations as a pior [15].

This regularization is performed in the space of distance maps (distance from camera to surface). The regularized distance map d_{rec} is computed as a weighted average of the distance map of the reconstructed surface from stereo endoscopic video d_{EV} with the distance map computed from the pre-operative CT segmentation d_{pre} at each pixel v:

$$d_{rec}(v) = [1 - \alpha(v)] d_{EV}(v) + \alpha(v) d_{pre}(v) \tag{3}$$

where

$$\alpha(v) = \exp\left[\frac{-\beta}{|d_{EV}(v) - d_{pre}(v)|}\right]$$

is an outlier-sensitive regularizer and $\beta > 0$ is a free variable that can be tuned to adjust the weight given to the pre-operative volume. This formulation gives a higher weight to d_{pre} when the difference between d_{pre} and d_{EV} is high (outliers).

(a) (b)

Fig. 3: Probabilistic segmentation of pre-operative CT scans of an *ex vivo* lamb kidney phantom with exophytic tumour: (a) original CT slice, and (b) corresponding probabilistic map of background (red), kidney (green), and tumour (blue).

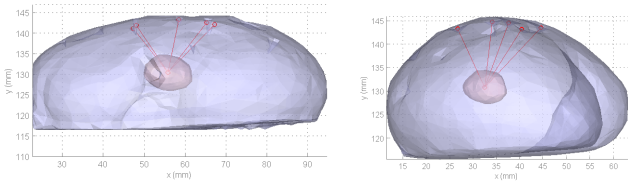

(a) (b)

Fig. 4: Our simulated kidney model (a) without external pressure, and (b) with simulated uniform external water pressure. The endophytic tumour (*purple mass*) is depicted inside the simulated kidney.

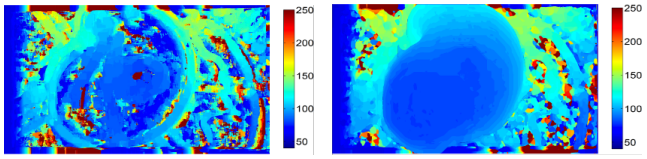

(a) (b)

Fig. 5: Distance maps (from camera to surface in mm) obtained from stereo surface reconstruction of a kidney phantom (a) without and (b) with regularization based on shape-prior.

B. Registration of Pre- and Intra-Operative Data

To register the pre-operative CT segmentation to the intra-operative stereo endoscopic view, we first perform a pose estimation, by manually providing 6 corresponding landmarks, which rigidly aligns the kidney and tumour segmented from the CT to the endoscopic video. Initial pose estimation is followed by an automatic registration step with rigid T_{rig} and deformable T_{def} transformation components that matches the probability map of the segmented pre-operative CT volume p_{pre} (Section II-A) to the probability map of the 3D stereo reconstructed surface p_{rec} (Section III-A) and of anatomical structures in the stereo images p_{stereo}. We calculate the pre-operative to intra-operative spatial transformation T by minimizing the following energy functional:

$$E(T; p_{pre}, p_{rec}, p_{stereo}) = \int_{3D} \mathcal{D}_1\Big(p_{rec}, p_{pre} \circ T\Big) + \kappa \int_{2D} \mathcal{D}_2\Big(p_{stereo}, \mathcal{P}\left(p_{pre} \circ T\right)\Big), \quad (4)$$

where $T = T_{def} \circ T_{rig}$ is the final transformation, $\mathcal{D}_1$ and $\mathcal{D}_2$ are dissimilarity measures between two probability maps, respectively in 3D and 2D, and $\mathcal{P}$ is the 3D to 2D projection function. $\kappa > 0$ is a constant that balances the contribution of image features and stereo reconstructed surface in the registration task.

IV. AUGMENTED REALITY VISUALIZATION

Finally, we present to the surgeon an augmented reality view showing an overlay of the tumour resection targets on top of the endoscopic view, in a way that depicts uncertainty in localizing the tumour boundary [16]. Our visual cues are derived from shape boundary uncertainties in the probabilistic segmentation of the pre-operative CT (Section II-A). We present two complimentary visualization methods, which give the surgeon the choice between a detailed view of uncertainties or a condensed view with minimal occlusion.

V. EXPERIMENTS

A. Materials

To evaluate our methods, we used data acquired from *in silico* and *ex vivo* phantoms for controlled experiments, as well as from real patients undergoing RAPN. An *in silico* cardiac phantom dataset[3] includes a low resolution stereo video (360×288 pixels), CT scans (512×512 pixels with 0.414 mm pixel spacing and 0.5 mm slice thickness), and ground truth data for stereo surface reconstruction [17], [18]. For more realistic controlled experiments, we acquired additional CT scans (512×512 pixels with 0.215 mm pixel spacing and 0.6 mm slice thickness) and high resolution stereo video (full HD 1080i resolution) of *ex vivo* lamb kidneys with artificial tumours and fiducials [15], [16]. We also collected patient data from 10 cases of RAPN including: pre-operative patient CT scans (Siemens CT Sensation 16 and 64 slices), and stereo endoscopic video at full HD 1080i (da Vinci Si HD, Intuitive Surgical, Inc.).

B. Results

The probabilistic segmentation with three classes (background, kidney, and tumour) was applied to pre-operative CT scans. An example result on an *ex vivo* lamb kidney is shown in Fig. 3. The simulation of deformations due to external pressure load showed a 29% improvement of tumour localization with respect to the kidney surface (Fig. 4), which we expect to significantly better estimate resection margins after insufflation of the patient [12]. The proposed stereo surface reconstruction method led to highly improved results [15], especially in poorly textured regions that mislead the dense matching (Fig. 5). The quality of the deformable registration of pre- and intra-operative data is illustrated in Fig. 6, showing the overlay of the kidney and tumour silhouette on the stereo endoscopic view. Note that the initial pose estimation does not need to be too close to the correct

[3]Available online http://hamlyn.doc.ic.ac.uk/vision/

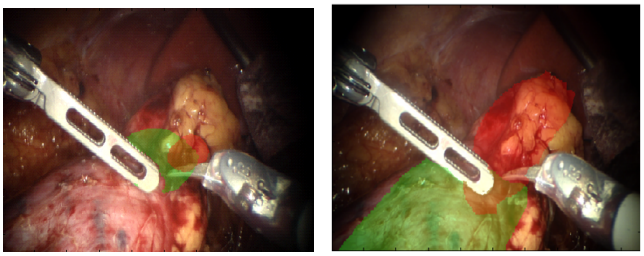

(a) (b)

Fig. 6: Fusion of pre-operative CT segmentation and stereo endoscopic view during RAPN (a) before and (b) after registration (kidney and tumour respectively in green and red).

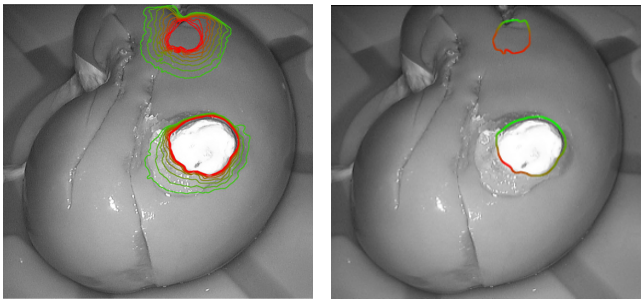

(a) (b)

Fig. 7: (a) Detailed and (b) simplified uncertainty-encoded visualization of endophytic (top) and exophytic (bottom) tumour boundaries in an *ex vivo* lamb kidney phantom.

pose. In fact, a rough estimation (Fig. 6a) is enough for our method to converge to a reasonable pose (Fig. 6b). As an end result provided to the surgeon, we show an augmented reality view of the kidney-tumour boundaries. Two solutions were proposed: a detailed visualization with several contours at different uncertainty levels (Fig. 7a) and a simplified visualization with a single color-coded contour (Fig. 7b) that provides similar information and does not obstruct too much the original view of the surgical scene [16].

VI. CONCLUSION

We developed a novel proof-of-concept framework for prior and uncertainty encoded augmented reality system that fuses pre-operative patient specific information into the intra-operative surgical scene. Preliminary studies and initial surgeons' feedback on the developed augmented reality system are encouraging. Our future work will focus on investigating the use of intra-operative ultrasound data in our system to leverage all imaging modalities available during surgeries, and the use of enhanced biomechanical models to better estimate soft tissue deformations that occur during the surgery.

ACKNOWLEDGMENT

This work was supported by NPRP Grant #4-161-2-056 from the Qatar National Research Fund (a member of the Qatar Foundation). The statements made herein are solely the responsibility of the authors.

REFERENCES

[1] I. S. Gill, L. R. Kavoussi, B. R. Lane, M. L. Blute, D. Babineau, J. R. Colombo, I. Frank, S. Permpongkosol, C. J. Weight, J. H. Kaouk, *et al.*, "Comparison of 1,800 laparoscopic and open partial nephrectomies for single renal tumors," *The Journal of urology*, vol. 178, no. 1, pp. 41–46, 2007.

[2] K. Cleary and T. M. Peters, "Image-guided interventions: technology review and clinical applications," *Annual review of biomedical engineering*, vol. 12, pp. 119–142, 2010.

[3] L.-M. Su, B. P. Vagvolgyi, R. Agarwal, C. E. Reiley, R. H. Taylor, and G. D. Hager, "Augmented reality during robot-assisted laparoscopic partial nephrectomy: Toward real-time 3D-CT to stereoscopic video registration," *Urology*, vol. 73, no. 4, pp. 896–900, 2009.

[4] S. Giannarou, M. Visentini-Scarzanella, and G. Yang, "Probabilistic tracking of affine-invariant anisotropic regions," *IEEE TPAMI*, 2013.

[5] P. Pratt, E. Mayer, J. Vale, D. Cohen, E. Edwards, A. Darzi, and G.-Z. Yang, "An effective visualisation and registration system for image-guided robotic partial nephrectomy," *Journal of Robotic Surgery*, pp. 1–9, 2012.

[6] Y. Otake, M. Armand, R. S. Armiger, M. D. Kutzer, E. Basafa, P. Kazanzides, and R. H. Taylor, "Intraoperative image-based multiview 2D/3D registration for image-guided orthopaedic surgery: Incorporation of fiducial-based C-arm tracking and GPU-acceleration," *IEEE TMI*, vol. 31, no. 4, pp. 948–962, 2012.

[7] O. Oktay, L. Zhang, P. Mansi, Tand Mountney, P. Mewes, S. Nicolau, L. Soler, and C. Chefdhotel, "Biomechanically driven registration of pre-to intra-operative 3D images for laparoscopic surgery," in *MICCAI*. Springer, 2013, pp. 1–9.

[8] N. Haouchine, J. Dequidt, I. Peterlik, E. Kerrien, M. Berger, and S. Cotin, "Image-guided simulation of heterogeneous tissue deformation for augmented reality during hepatic surgery," in *ISMAR*, 2013.

[9] L. Grady, "Random walks for image segmentation," *IEEE TPAMI*, vol. 28, no. 11, pp. 1768–1783, 2006.

[10] Grady, "Multilabel random walker image segmentation using prior models," *CVPR*, vol. 1, pp. 763–770, 2005.

[11] V. Egorov, S. Tsyuryupa, S. Kanilo, M. Kogit, and A. Sarvazyan, "Soft tissue elastometer," *Medical engineering & physics*, vol. 30, no. 2, pp. 206–212, 2008.

[12] I. Figueroa, J.-M. Peyrat, G. Hamarneh, and R. Abugharbieh, "Biomechanical kidney model for predicting tumor displacement in the presence of external pressure load," in *IEEE ISBI*, 2014.

[13] S. Bernhardt, J. Abi-Nahed, and R. Abugharbieh, "Robust dense endoscopic stereo reconstruction for minimally invasive surgery," *MICCAI Workshop on Medical Computer Vision (MCV)*, pp. 198–207, 2012.

[14] F. Islam, A. Amir-Khalili, J.-M. Peyrat, J. Abi-Nahed, A. Al-Ansari, and R. Abugharbieh, "Real-time GPU implementation of correlation-based dense matching of stereo endoscopic images for surface reconstruction," in *Qatar Foundation Annual Research Conference*, 2013.

[15] A. Amir-Khalili, J.-M. Peyrat, G. Hamarneh, and R. Abugharbieh, "3D surface reconstruction of organs using patient-specific shape priors in robot-assisted laparoscopic surgery," in *MICCAI Workshop on Computational and Clinical Applications in Abdominal Imaging*, 2013, vol. LNCS 8198, pp. 184–193.

[16] A. Amir-Khalili, M. S. Nosrati, J.-M. Peyrat, G. Hamarneh, and R. Abugharbieh, "Uncertainty-encoded augmented reality for robot-assisted partial nephrectomy: A phantom study," in *MICCAI Workshop on Medical Imaging and Augmented Reality (MIAR)*, 2013, vol. LNCS 8090, pp. 182–191.

[17] D. Stoyanov, D. M. V. Scarzanella, P. Pratt, and G.-Z. Yang, "Real-time stereo reconstruction in robotically assisted minimally invasive surgery," in *MICCAI*, 2010, vol. LNCS 6361, pp. 275–282.

[18] P. Pratt, D. Stoyanov, M. Visentini-Scarzanella, and G.-Z. Yang, "Dynamic guidance for robotic surgery using image-constrained biomechanical models," in *MICCAI*, 2010, vol. LNCS 8090, pp. 77–85.